Digital Image Information Extraction Techniques for Snow Cover Mapping from Remote Sensing Data

Chapter · January 2011

DOI: 10.1007/978-90-481-2642-2_498

3 authors, including:

Aparna Shukla
Wadia Institute of Himalayan Geology
25 PUBLICATIONS **184** CITATIONS

SEE PROFILE

Krabill, W., Thomas, R., Jezek, K., Kuivinen, K., and Manizade, S., 1995. Greenland ice sheet thickness changes measured by laser altimetry. *Geophysical Research Letters*, **22**(17), 2341–2344.
Liu, H. X., Jezek, K. C., Li, B. Y., 1999. Development of an Antarctic digital elevation model by integrating cartographic and remotely sensed data: a geographic information system based approach. *J Geophys Res-Solid Earth*, **104**, 23199–23213.
Lodwick, G. H., and Paine, S. H., 1985. A digital elevation model of the Barnes Ice-Cap Derived from Landsat-MSS Data. *Photogrammetric Engineering and Remote Sensing*, **51**(12), 1937–1944.
Magnússon, E., Björnsson, H., Pálsson, F., and Dall, J., 2005. The 20th century retreat of ice caps in Iceland derived fromairborne SAR: W-Vatnajökull and N-Mýrdalsjökull. *Earth and Planetary Science Letters*, **237**, L05504.
Muskett, M. M., Lingle, C. S., and Rabus, B. T., 2003. Multidecadal elevation changes on Bagley Ice Valley and Malaspina Glacier, Alaska. *Geophysical Research Letters*, **30**(16), 1857-1–1857-4.
Reinhardt, W., Rentsch, H., 1986. Determination of changes in volume and elevation of glaciers using digital elevation models for the Vernagtferner, Ötztal Alps, Austria. *Ann Glaciol*, **8**, 151–155.
Rémy, F., Legrésy, B., and Testut, L., 2001. Ice sheets and satellite altimetry. *Surveys in Geophysics*, **22**(1), 1–29.
Rippin, D., Willis, I., Arnold, N., Hodson, A., Moore, J., Kohler, J., and BjöRnsson, H., 2003. Changes in geometry and subglacial drainage of Midre Lovénbreen, Svalbard, determined from digital elevation models. *Earth Surface Processes and Landforms*, **28**(3), 273–298.
Robin, G., and de, Q., 1966. Mapping the Antarctic ice sheet by satellite altimetry. *Canadian Journal of Earth Sciences*, **3**(6), 893–901.
Rosen, P. A., Hensley, S., Joughin, I. R., Li, F. K., Madsen, S. N., Rodríguez, E., and Goldstein, R. M., 2000. Synthetic aperture radar interferometry. *Proceedings of the IEEE*, **88**(35), 333–382.
Rosmorduc, V., Benveniste, J., Lauret, O., Maheu, C., Milagro, M., and Picot, N., 2009. *Radar altimetry tutorial*. In Benveniste, J., and Picot, N. (eds.), http://www.altimetry.info
Scambos, T. A., and Fahnestock, M. A., 1998. Improving digital elevation models over ice-sheets using AVHRR-based photoclinometry. *Journal of Glaciology*, **44**(146), 97–103.
Scambos, T. A., and Haran, T. M., 2002. An image-enhanced DEM of the Greenland ice sheet. *Annals of Glaciology*, **34**, 291–298.
Thomas, R. H., Rignot, E., Casassa, G., Kanagaratnam, P., Acuña, C., Akins, T., Brecher, B., Frederik, E., Goginini, P., and Krabill, W., 2004. Accelerated sea-level rise from West-Antartica. *Science*, **306**(5694), 255–258.
Toutin, Th., 2001. Elevation modelling from satellite visible and infrared (VIR) data: a review. *International Journal of Remote Sensing*, **22**(6), 1097–1125.
Toutin, Th., and Gray, A. L., 2000. State-of-the-art of extraction of elevation data using satellite SAR data. *ISPRS Journal of Photogrammetry and Remote Sensing*, **55**(1), 13–33.
Welch, R., Jordan, R. T., Lang, H., and Murakani, H., 1998. ASTER as a source for topographic data in the late 1990s. *IEEE Transactions on Geoscience and Remote Sensing*, **36**(4), 1282–1289.
Wingham, D., 1995. The limiting resolution of ice-sheet elevations derived from pulse-limited satellite altimetry. *Journal of Glaciology*, **41**(138), 414–422.
Zwally, H. J., Schutz, B., Abdalati, W., Spinhirne, J. D., Bentley, C., Brenner, A., Bufton, J., Dezio, J., Hancock, D., and Harding, D., 2002. ICESat's laser measurements of polar ice, atmosphere, ocean and land. *Journal of Geodynamics*, **34**(3–4), 405–445.

Cross-references

Automated Glacier Mapping
Glacier Mass Balance
Glacier Motion/Ice Velocity
GRACE in Glaciology
Greenland Ice Sheet
Ground Penetrating Radar Measurements Over Glaciers
Ice Sheet Mass Balance
ICESat Data in Glaciological Studies
LIDAR in Glaciology
Optical Remote Sensing of Alpine Glaciers
Synthetic Aperture Radar (SAR) Interferometry for Glacier Movement Studies

DIGITAL IMAGE INFORMATION EXTRACTION TECHNIQUES FOR SNOW COVER MAPPING FROM REMOTE SENSING DATA

Manoj K. Arora[1], Aparna Shukla[2], Ravi P. Gupta[3]
[1]Department of Civil Engineering, Indian Institute of Technology Roorkee, Roorkee, India
[2]Uttarakhand Space Application Centre, Dehradun, India
[3]Department of Earth Sciences, Indian Institute of Technology Roorkee, Roorkee, India

Definition

Digital image information extraction. A set of image-processing techniques applied to the satellite images in digital form for the enhancement and extraction of the required information.
Snow-cover mapping from remote sensing data. Mapping of the snow-covered areas in the satellite image by application of the specialized digital image information extraction techniques.

Introduction

Snow is one of the most sensitive and vital natural resources. Over the years, gradual technological progress in mapping of snow-covered areas using remote sensing data has been influenced by several interrelated factors. These include advancements in the satellite sensor and image-processing technologies, and increasing demand for accurate and frequent monitoring of snow-covered areas due to mounting pressures from rapid industrialization, urbanization, and changing climate. Thus, regular and precise mapping of snow-covered regions is important at various scales due to several reasons such as:

1. On global and continental scales, snow due to its highly reflective nature and large surface coverage (snow can cover up to 40% of the Earth's land surface during the Northern Hemisphere winter) has great impact on climate variations, surface radiation balance, and energy exchange (Wang and Li, 2003).
2. On a regional scale, snow cover estimates constitute the primary input parameter for hydrological modeling

(Rango and Martinec, 1981; Shiyin et al., 2003; Fukushima et al., 1991).
3. On a local scale, accurate estimates of snow cover areas form key inputs to the mass balance studies, volumetric estimates, meltwater runoff modeling and snow hazard prediction modeling (Haeberli et al., 1998 and 2001; Berthier et al., 2007; Oerlemans et al., 2007; Quincey et al., 2005; Khromova et al., 2006; IPCC, 2007; Kulkarni et al., 2007).

Remote sensing data acquired in relevant parts of the electromagnetic spectrum have been widely employed for mapping of snow-covered area throughout the world (Konig et al., 2001; Hall et al., 2005; Bamber, 2006). Present status of snow-cover mapping can broadly be described based on:

1. The scale of mapping (small, medium, or large) both at pixel and sub-pixel levels
2. The region of electromagnetic spectrum utilized, namely, ultraviolet, visible, infrared, or microwave (active or passive)
3. The type of sensor used (Landsat TM and ETM+, SPOT VGT, NOAA AVHRR, IRS LISS-III, IV, Terra MODIS and ASTER, etc.)
4. The image information extraction techniques employed on remote sensing data

The aim of this chapter is to review the status of snow-cover mapping based on image information techniques. First, the conventional techniques of snow-cover mapping have been reviewed and their limitations highlighted, which are followed by a discussion on the importance of remote sensing in mapping of snow cover. A number of digital image information techniques employed for mapping of snow-covered areas, till date, have been conversed.

Conventional approaches of snow-cover mapping

Traditionally, snow cover has been mapped using ground (Potts, 1944; Miller, 1953) and aerial photographic surveys. Ground surveys may not be as complete as aerial surveys because of the field of vision and other obstructions, such as hills. Aerial photographic surveys provide more comprehensive information of the snow cover as compared to the ground surveys. It, however, also has some limitations such as time required to process a large number of photographs covering a big basin, high costs of operation of the aircraft, and difficulty in interpretation of snow cover in the forested areas (Singh and Singh, 2001). Further, reliability of the snow cover estimates from extrapolation of the snow cover information from meteorological stations depends heavily on the density of the weather stations, which is often quite insufficient. The temperature lapse-rate method for snow cover area approximation ignores the snow cover area lying outside the glacier and assumes snow, glacial ice, and debris-covered glacial ice as one homogeneous body.

Remote sensing for snow-cover mapping

In view of the vastness, inaccessible nature and harsh climatic conditions of the snow-covered areas, remote sensing is perhaps the most effective tool for comprehensive and repetitive study of these areas in a cost-effective manner. The remote sensing data can be obtained at a range of spectral, spatial, and temporal resolutions, which make them suitable for snow-cover mapping and monitoring. In fact, the high albedo of snow presents a high contrast with most other land cover types (except clouds) and for this reason maps of snow-covered area were one of the first products of satellite remote sensing (Tarble, 1963).

Understanding of spectral characteristics of snow forms an important prerequisite in its mapping from the satellite remote sensing data. Significant studies on the reflective properties of snow have been done by Wiscombe and Warren (1980), Warren and Wiscombe (1980), Warren (1982), and Zeng et al. (1984). Discussion of factors influencing snow reflectance have been given by Foster et al. (1987), Winther and Hall (1999), and Winther et al. (1999). As shown in Figure 1, snow reflectance is very high in the visible and much lower in the infrared region of the electromagnetic spectrum. Reflectance of snow is influenced by various factors such as grain size, contamination, solar zenith angle, cloud cover, metamorphism and age factor, and liquid water content.

In visible wavelengths (400–700 nm), snow reflectance is quite sensitive to minor amounts of contamination like carbon soot, volcanic ash, continental dust, etc. In the near- and middle-infrared region (700–3,000 nm), snow reflectance is sensitive to the grain size. The metamorphism of the snow cover, in general, results in a decrease of reflectance. Liquid water content in the snowpack has the effect of increasing the effective grain size and thus lowering the snow albedo (Konig et al., 2001).

Reflectance of snow is anisotropic and dependent on incidence and view angle. This dependence is described by the bidirectional reflectance distribution function (BRDF) (Knap and Reijmer, 1998). However, most satellite-derived albedo studies have generally not taken into account the anisotropic reflectance behavior of snow. The effect of anisotropic reflection increases as snow metamorphoses, for example, with increasing grain size and surface melt-freeze processes that sometimes produce a highly specular surface ("firnspiegel") (Konig et al., 2001).

Recently, there have been several commendable attempts to employ satellite remote sensing for mapping and monitoring of some major characteristics (such as area, depth, volume, and albedo) of snow as these constitute vital input parameters for hydrological, climatological, and hazard prediction models. Though, remote sensing greatly facilitates the mapping and monitoring of snow cover. However, mapping snow cover from remotely sensed data may also be fraught with a number of snags, which may be data and technology dependent. The main problem with data from visible and near-infrared sensors is their weather dependency (e.g., influence of the

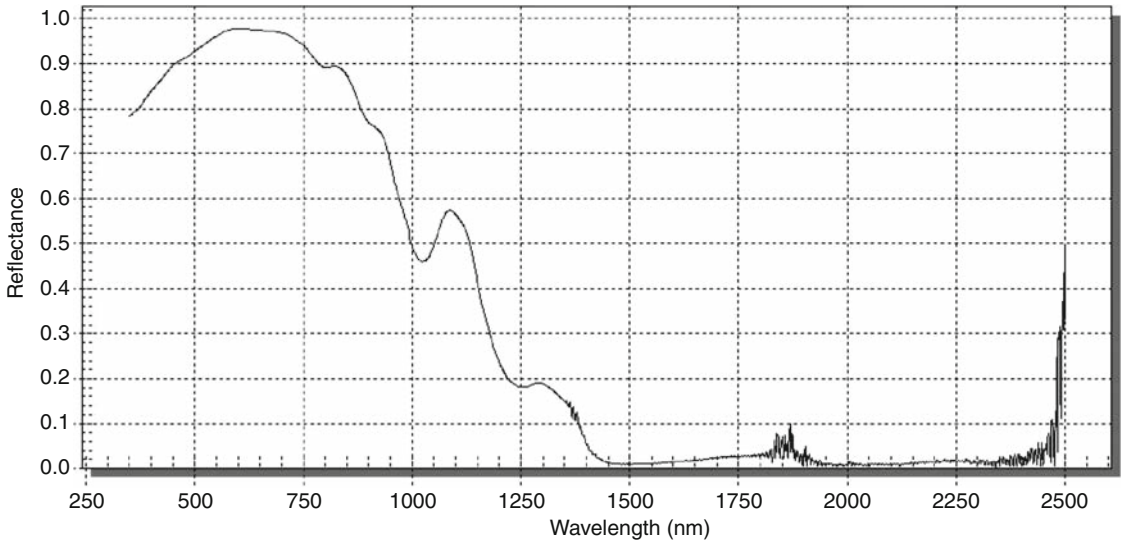

Digital Image Information Extraction Techniques for Snow Cover Mapping from Remote Sensing Data, Figure 1 Ground-based spectral reflectance curve of snow.

atmosphere on these data, especially the existence of cloud cover). A number of approaches have been suggested to get over the problem of cloud cover. Utilization of active and passive microwave data may overcome this problem. However, passive microwave data underestimates snow cover, perhaps due to their inability to map snow cover under forest and to distinguish wet snow from surrounding terrain. Basin-wide or large-scale snow and ice mapping has also been attempted using active microwave data obtained through Synthetic Aperture Radar (SAR) sensors since these sensors can discriminate between snow and bare ground at a spatial resolution that is compatible with topographic variation in mountainous basins. However, SAR data suffers from several limitations such as difficulties in interpretation of the recorded backscatter (Konig et al., 2001), complex image-processing requirements, and problems in distinguishing between wet snow and other smooth surfaces (Shi and Dozier, 1997). Data from different regions of the electromagnetic spectrum have also been used in combination for snow-cover mapping (Tait et al., 1999; Solberg et al., 2005; Liang et al., 2008).

Mountain shadows are also impediment to the determination of the snow line or the extent of snow-covered areas of a basin, especially in steep mountain terrains. A way out may be to combine the visible data with terrain features to minimize the effect of shadow. Alternatively, a number of ratio images and spectral indices may also be devised to map the snow cover extent (Dozier, 1989; Hall et al., 1995b).

Another problem faced in mapping of snow cover is the forest cover. A major part of the snow falling over forested areas reaches the ground after filtering through the forest canopy. Depending on the forest density, a part of fresh snowfall may stay atop the forest canopy. A dense forest cover may obscure underlying snow. Therefore, much attention is being paid to effectively determine snow-covered areas in forested regions (Klein et al., 1998; Vikhamar and Solberg, 2002, 2003; Shimamura et al., 2006). These include, using some vegetation indices such as the Normalized Difference Vegetation Index (NDVI) (Klein et al., 1998), formulating special indices for mapping snow cover under forests by using the near-infrared band (Shimamura et al., 2006) and by utilizing spectral signatures of snow cover under forests separately (Vikhamar and Solberg, 2002, 2003).

It is thus clear that mapping snow cover from remote sensing data is an intricate task and requires effective digital image information extraction techniques to extract these from a variety of aircraft- and satellite-based data acquired at varied spectral, spatial, and temporal resolutions. The use of ancillary data in this process may also not be undermined.

Digital image information extraction techniques for snow-cover mapping

A number of image information extraction techniques have been developed in view of the increasing demands for improved areal estimates of snow cover for varied applications. These techniques, as discussed in the next section, may be categorized as:

1. Manual delineation
2. Change detection–based method
3. Spectral ratios
4. Spectral indices
5. Per pixel image classification
6. Sub-pixel image classification

In order to demonstrate the implementation of these techniques and their comparison, results from a case study in mapping snow cover in a test glacier located in the Chenab basin, Western Himalaya, India, have also been presented.

Manual delineation

Manual delineation involves on-screen digitization of the satellite images based on the visual interpretation of snow-covered areas using a set of interpretation elements namely tone, texture, shape, size, association, pattern, and shadow applied individually or in combination. It has been widely used for mapping of glacial ice and snow extents, and in particular, for the estimation of retreat and deglaciation in various parts of the world (Hall et al., 1995a; Williams et al., 1997; Williams and Hall, 1993; Khromova et al., 2006; Kulkarni et al., 2007). Though being effective, the manual delineation is a very tedious and time-consuming task and may not be appropriate for mapping at operational level. Moreover, since the technique involves high degree of subjectiveness, therefore results from different sources may seldom match due to varying degrees of accuracy and bias involved.

Change detection–based method

In the change detection–based method, a snow-free satellite image is used as a reference image and is digitally compared, pixel by pixel, to record snow and non-snow-covered pixels. The brightness of the images may have to be adjusted to account for the daily and seasonal solar illumination angle differences. This method was developed initially by the U.S National Weather Station (NWS) for operational snow-cover mapping with AVHRR and Geostationary Environmental Satellite (GOES) sensors (Allen and Mosher, 1985; Holroyd et al., 1989). The method was found suitable for identification of snow in coniferous forested areas (Baumgartner and Rango, 1991). A variant of this change detection method was developed by Lillesand et al. (1982), which accounted for the inherent variations within cover types, for between-date variations within similar cover types, and for differing site characteristics (Baumgartner and Rango, 1991).

Spectral ratios

Formation of spectral ratios involves pixel-by-pixel division of the two bands of an image, which are selected in such a way that these maximize the spectral contrast between snow cover and other classes. The ratio image is then segmented using appropriate threshold values for mapping the snow cover. Band ratioing has been found to be a useful method for enhancing snow cover features in the multispectral images (e.g., Hall et al., 1987, 1988; Jacobs et al., 1997; Paul et al., 2004; Boresjö Bronge and Bronge, 1999; Williams et al., 1991). It has also been used to reduce the variable effects of solar illumination and topography besides enhancing the spectral information in the images (Justice et al., 1981; Gupta, 2003). The bands used to create ratios for mapping of snow-covered areas rely on its fundamental spectral characteristics, that is, high reflectance in visible region and strong absorption in the infrared region of the electromagnetic spectrum. Some typical spectral ratios for snow-cover mapping as cited in the literature have been compiled in Table 1.

Hall et al. (1987) used the ratio of TM4 (NIR) and TM5 (SWIR) bands to characterize snow and ice zones on glaciers using their spectral properties. Ratio values of raw Digital Numbers (DNs) (i.e., spectral response of pixels) were thresholded to generate a glacier mask by Hall et al. (1988). Rott and Markl (1989) found that spectral ratio TM3/TM5 revealed better results in shadowed areas than those obtained from TM4/TM5, whereas the latter showed better performance in mapping glacier areas facing the sun.

Jacobs et al. (1997) used atmospherically corrected spectral reflectance images obtained from TM4/TM5 and TM3/TM5, respectively, to obtain glacier mask after thresholding. Williams et al. (1991) found the TM4/TM5 ratio to be useful for discriminating glacier facies for temperate glaciers. Boresjö Bronge and Bronge (1999) found that the TM3/TM4 ratio resulted in the most accurate discrimination between blue ice and other snow types. Further, this ratio was also insensitive to the influence of thin clouds and cloud shadows. Paul (2000), while comparing various methods for glacier mapping using Landsat TM data, found that segmentation of a ratio image (TM4/TM5) with raw DNs yielded accurate glacial mapping.

Digital Image Information Extraction Techniques for Snow Cover Mapping from Remote Sensing Data, Table 1 Basic formulations of spectral ratios for snow-cover mapping

S.No.	Popular name	Formulation	Used by
1	*TM4/TM5*	$\frac{\text{NearInfrared(NIR)}}{\text{ShortwaveInfrared(SWIR)}}$	Hall et al. (1987, 1988); Rott and Markl (1989); Jacobs et al. (1997); Williams et al. (1991); Bronge and Bronge (1999); Paul (2000, 2003); Paul et al., (2002, 2004).
2	*TM3/TM5*	$\frac{\text{Red}}{\text{ShortwaveInfrared(SWIR)}}$	Rott and Markl (1989); Jacobs et al. (1997); Bronge and Bronge (1999).
3	*TM3/TM4*	$\frac{\text{Red}}{\text{NearInfrared(NIR)}}$	Bronge and Bronge (1999).

For demonstrating the snow mapping capabilities of spectral ratios, the most widely used NIR/SWIR ratio was selected in the study conducted in Chenab basin (Figure 2) and was applied to an IRS P6 AWiFS (Advanced Wide Field Sensor) image of the test glacier. The histogram of NIR/SWIR ratio image (Figure 2c) was studied for the determination of an appropriate threshold value. Snow-ice binary glacier terrain maps were generated using arbitrary thresholds of 1.5 and 2.0 (commonly used threshold; Paul, 2003) (Figure 2d and 2e, respectively). It can be seen that the ratio is unable to segregate the snow and ice class and fail to map the mixed ice and debris (MID) and supraglacial debris (SGD) classes (encircled areas in Figure 2a, 2d and 2e) toward the glacier snout. Thus, although spectral ratioing constitutes a fast and robust method for mapping snow- and ice-covered areas, the subjectivity involved in the derivation of appropriate thresholds and its inability to precisely differentiate between snow and ice zones limit its use.

Spectral indices

Besides the ratios, several empirical spectral indices have also been devised (Dozier, 1989; Hall et al., 1995b; Xiao et al., 2001; Shimamura et al., 2006; Keshri et al., 2009) for segregation and mapping of the snow and ice classes. Some of these spectral indices, their utility, and cited reference have been compiled in Table 2. Spectral indices characterize the basic spectral differences in the classes to be separated as well as assist in diminishing the radiometric effects of differential solar illumination and topography.

Normalized Difference Snow Index (NDSI), as defined in Table 2, was formulated by Dozier (1989) and Hall et al. (1995b). The basis of index is the high reflectance of snow in the visible region and a very low reflectance in the SWIR region, thereby providing high values of NDSI for snow-covered areas (Hall et al., 1995b; Nolin and Liang, 2000).

The main advantages of using NDSI are:

1. Discrimination between snow and clouds
2. Removal of mountain shadows to some extent

Winther and Hall (1999) used NDSI for snow cover area estimation to provide input for hydrological models for snow runoff modeling. Wang and Li (2003) compared NDSI with other methods and found it to be a valid and rational method for extracting snow cover areas. Kulkarni et al. (2006) employed an NDSI-based algorithm for producing snow cover products (5- and 10-day products) using data from IRS-P6 AWiFS sensor in Himalayan region.

MODIS snow-cover mapping algorithm referred as SNOWMAP is also based on the NDSI with few additional thresholds. SNOWMAP is a computationally frugal algorithm and thus is simple to implement at global scale (Hall et al., 1995b; Riggs et al., 1994; Riggs et al., 1996; Hall et al., 1998; Klein et al., 1998).

On similar lines, Xiao et al. (2001) proposed the Normalized Difference Snow and Ice Index (NDSII-1) (Table 2) for mapping snow and ice cover utilizing VEGETATION (VGT) sensor of SPOT 4. For Landsat TM data, they found that NDSII-1 yielded almost similar results as compared to NDSI. Later, NDSII-1 has also been used by them for spatial and temporal analysis of snow and ice cover over Asia and pan-Arctic zone using multi-temporal VGT sensor data.

Gupta et al. (2005) utilized NDSI along with a DEM for mapping dry and wet snow using IRS LISS-III data. The results (the area covered by dry snow) of this method were validated and compared with the area of non-melting zone from the temperature lapse method. The two were found to be in close correspondence (i.e., differences were $<15\%$).

Shimamura et al. (2006) intercompared NDSI with another index S3 (initially proposed by Saito and Yamazaki (1999) for GLI sensor of ADEOS) using Landsat ETM + data and found that S3 index was advantageous for mapping snow cover under dense forests. They argued that similar to other studies while the S3 index (calculated using red, NIR, and SWIR bands) was able to map snow cover under forested areas without any reference data (e.g., NDVI image), the NDSI could not.

Keshri et al. (2009) have recently proposed two indices (Normalized Difference Glacier Index (NDGI) and Normalized Difference Snow and Ice Index (NDSII-2)) for detailed mapping of supraglacial terrain. The indices facilitate three-step discrimination. First, the snow and ice are separated from rest of the terrain using NDSI, then snow and ice from ice-mixed-debris class using NDGI, and finally snow from ice using NDSII-2.

For the case study in Chenab basin, an NDSI image was created using Green and SWIR bands of the IRS P6 – AWiFS image of the test glacier. Thereafter, its frequency distribution (Figure 3c) was analyzed and two binary glacier terrain maps (Figure 3d and 3e) were generated at 0.4 (commonly used thresholds, Dozier, 1989; Hall et al., 1995b) and 0.5 thresholds. It can be seen that on increasing the threshold value from 0.4 to 0.5 for reducing the misclassification of glacial lake water, the ice area near the snout also diminishes (Figures 3d and e). Thus, creation of empirical spectral indices, such as NDSI, may assist in quick segregation of snow and ice classes from the rest of the classes under various terrain conditions (e.g., shadow, highly rugged topography, and forest cover). However, selection of an appropriate threshold value is a crucial task, as even a slight variation in threshold values may lead to over- or underestimation of snow cover. Moreover, the thresholds may vary with different satellite sensors as well as seasons (Dozier, 1989, Hall et al., 1995b).

Digital image classification

Digital image classification is perhaps the major image-processing task for extracting useful information from remote sensing data. The aim is to produce thematic maps where each pixel in the image is assigned a class (e.g., snow) on the basis of its spectral response to produce a classification. The per-pixel (PP) classification is

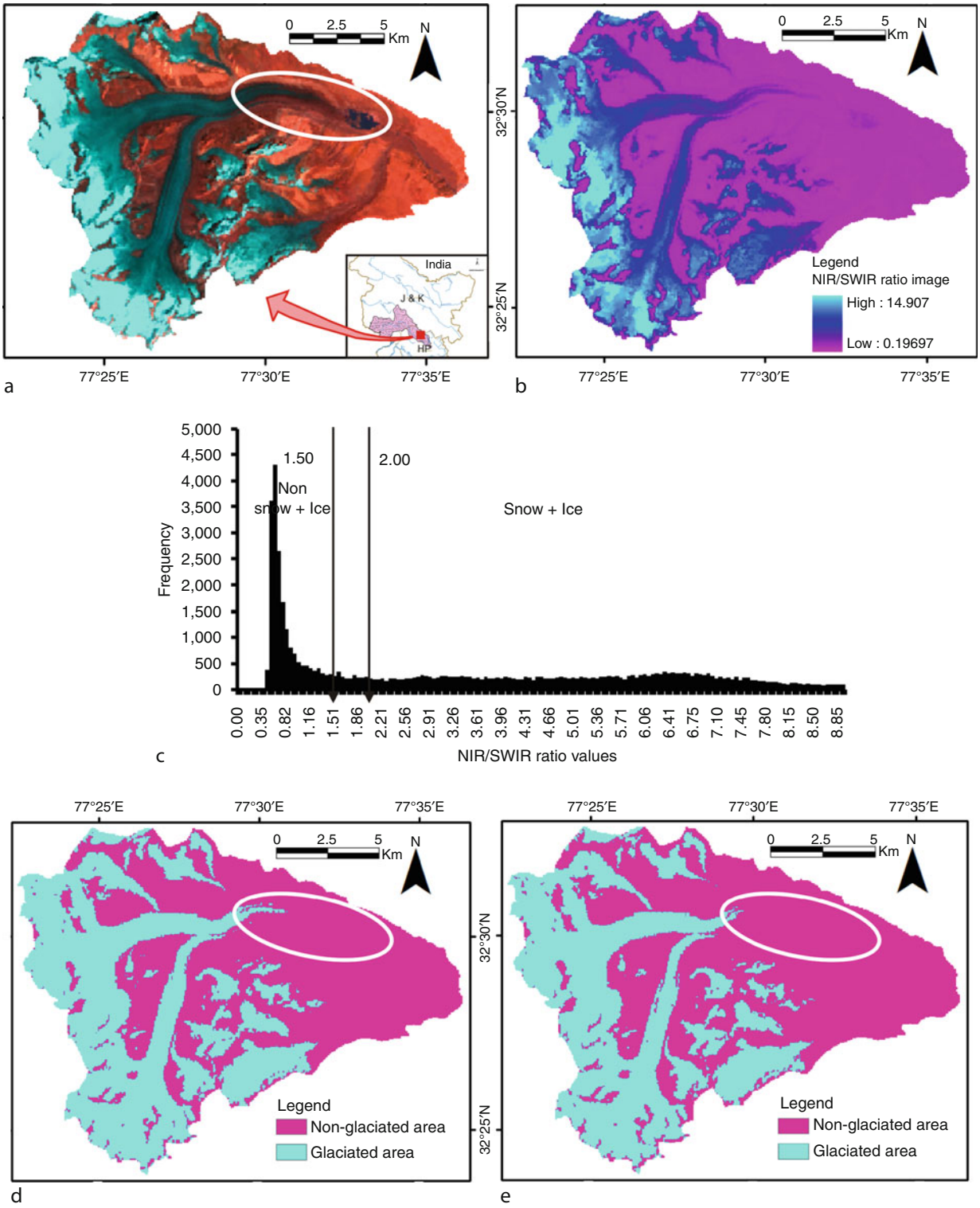

Digital Image Information Extraction Techniques for Snow Cover Mapping from Remote Sensing Data, Figure 2 Snow-cover mapping using NIR/SWIR ratio. **(a)** An FCC (R = B5, G = B4, B = B3) of AWiFS image of a test glacier, **(b)** NIR/SWIR ratio image, **(c)** histogram of NIR/SWIR image, and **(d)** and **(e)** binary glacier terrain maps derived from NIR/SWIR ratio image at 1.5 and 2.0 threshold values.

Digital Image Information Extraction Techniques for Snow Cover Mapping from Remote Sensing Data, Table 2 Formulations and utility of various spectral indices

Name of the index	Cited reference	Formulation	Utility
Normalized Difference Snow Index (NDSI)	Dozier (1989), Hall et al. (1995b)	$\text{NDSI} = \frac{\text{Green} - \text{SWIR}}{\text{Green} + \text{SWIR}}$	For mapping and differentiation of snow-ice covered areas from non-snow and ice areas.
Normalized Difference Snow and Ice Index (NDSII-1)	Xiao et al. (2001)	$\text{NDSII} = \frac{\text{Red} - \text{SWIR}}{\text{Red} + \text{SWIR}}$	For mapping and differentiation of the snow-ice covered areas from non-snow and ice areas.
S3 Index	Shimamura et al. (2006)	$\text{S3} = \frac{\text{NIR}(\text{red} - \text{SWIR})}{(\text{NIR} + \text{red})(\text{NIR} + \text{SWIR})}$	For mapping snow and ice cover under forest covered areas.
Normalized Difference Glacier Index (NDGI)	Keshri et al. (2009)	$\text{NDGI} = \frac{\text{Green} - \text{Red}}{\text{Green} + \text{Red}}$	For mapping and differentiating between snow-ice and mixed ice and debris class.
Normalized Difference Snow and Ice Index (NDSII-2)		$\text{NDSII} = \frac{\text{Green} - \text{NIR}}{\text{Green} + \text{NIR}}$	For mapping and differentiating between snow and ice class.

suitable when the image pixels are pure (i.e., one pixel area is covered by a single class). However, as the spatial resolution becomes coarser, the proportion of mixed pixels (i.e., pixels containing more than one class) increases, which leads to erroneous per-pixel classification. Therefore, sub-pixel classification has been suggested. The output from a sub-pixel (SP) classification is set of fraction images (equal to the number of classes being mapped) each depicting spatial extent of a class. Both supervised and unsupervised approaches can be used to produce per-pixel and sub-pixel classifications.

Supervised classification is one of the most widely used one in various remote sensing studies, and involves four stages, as depicted in Figure 4. The salient characteristics of some of the supervised and unsupervised classifiers are given in Table 3. The following section focuses on the review of per-pixel image classifiers for mapping snow cover.

Snow-cover mapping using per-pixel image classification

Della Ventura et al. (1983) developed a technique for automatic glacier-cover mapping (i.e., mapping of ice, snow, and other classes) using Landsat MSS data. Later, Della Ventura et al. (1987) applied a decision tree classifier and achieved more accurate results than the previous attempt. A supervised maximum-likelihood classification was applied to Landsat MSS and TM scenes by Gratton et al. (1990) to map seven classes. However, in that study, misclassification between clouds, shadows, and water, particularly in debris-covered glaciers, was observed due to which the maps had to be corrected manually. An inventory of the entire Southern Patagonian Icefield (SPI) based on TM data of year 1986 was prepared by Aniya et al. (1996) using cluster analysis (ISODATA) of TM bands 1, 4, and 5 to produce three classes (snow, ice, and rock). A parallelepiped classification was performed. In case of misclassification between ice in shade and supraglacial till, manual correction was applied (Paul, 2003).

The fuzzy set theory was used by Binaghi et al. (1997) for glacier classification. Although, a high classification accuracy was achieved, the method being technically intensive, was quite complex and moreover, debris cover on glaciers could not be mapped (Paul, 2003).

Ehrler and Seidel (1995) developed an algorithm for mapping snow and ice areas using Landsat TM and MSS and SPOT XS data via supervised classification for snow runoff modeling (SRM). The images were segmented into four illumination classes depending on the local incidence angle. Each illumination class was separately classified into bare ice, snow, transition zone, and snow free (aper). Wang and Li (2003) also performed supervised classification of images from Landsat TM, Terra MODIS, and NOAA-AVHRR to map three classes (old snow, fresh snow, and firn) using minimum distance classifier and intercompared with other snow and ice mapping techniques.

Additional information from sources other than spectral data (such as transformed spectral bands, DEM, and its derivatives) have also been utilized in the supervised classification process by some researchers either to simply augment the snow cover classifications (Boresjö Bronge and Bronge, 1999; Sidjak and Wheate, 1999).

Boresjö Bronge and Bronge (1999) applied supervised MLC to the principal components (PCs) of Landsat TM image for mapping blue ice of different characteristics as well as snow with various degrees of metamorphism. Although, the major snow and ice classes could be discerned, snow misclassifications were observed for image pixels covered with clouds and shadows. Sidjak and Wheate (1999) applied the supervised MLC using different input bands (PCs, TM4/TM5 ratio, NDSI, TM543 composite image) for mapping the glacier extent and discriminating glacier zones. The approach was able to

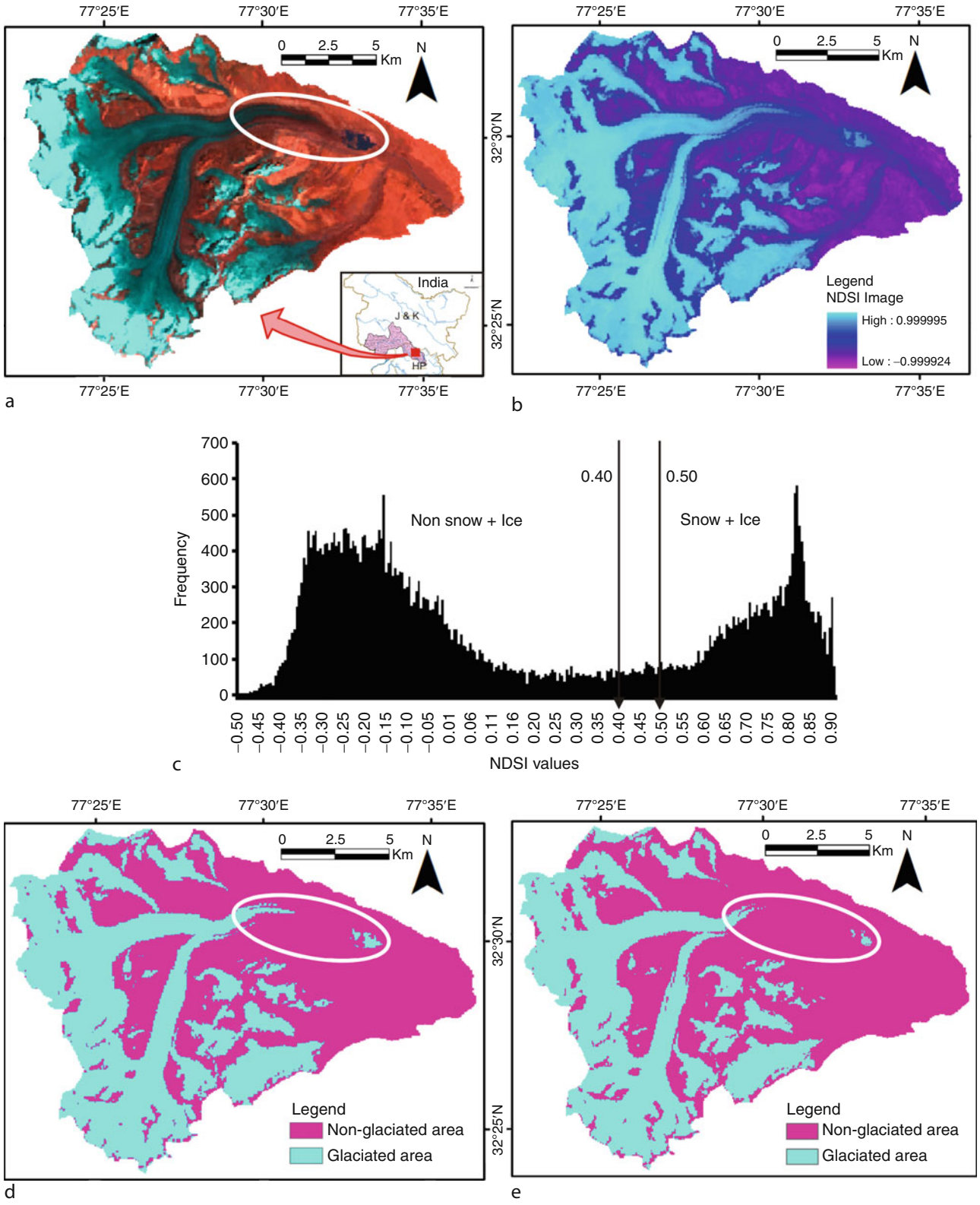

Digital Image Information Extraction Techniques for Snow Cover Mapping from Remote Sensing Data, Figure 3 Snow-cover mapping using NDSI. **(a)** FCC (R = B5, G = B4, B = B3) of AWiFS image, **(b)** NDSI image, **(c)** histogram of NDSI image, and **(d)** and **(e)** binary glacier terrain maps derived from NDSI ratio image at 0.4 and 0.5 thresholds.

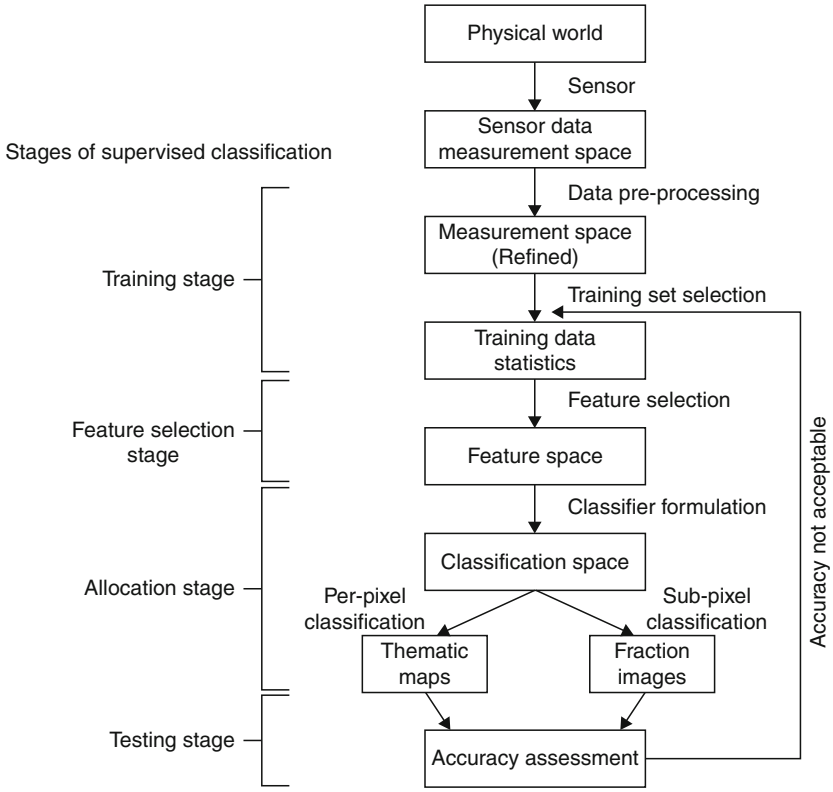

Digital Image Information Extraction Techniques for Snow Cover Mapping from Remote Sensing Data, Figure 4 Typical flowchart of a supervised classification process (Modified after Gupta, 2003).

accommodate problems of sensor saturation and shadowed areas, and thus refining the discrimination of debris-mantled ice and ice marginal water bodies.

In order to assess the influence of ancillary data together with spectral data and their transformations in the classification process, snow-cover mapping in Chenab basin was carried out using AWiFS image via MLC. Use of three different datasets, namely, only reflectance data, reflectance data + NDSI, and reflectance data + thermal data (ASTER TIR data), was made in the classification to produce three glacier terrain maps of the area (Figure 5). Comparing these maps those produced from other snow-cover mapping methods, it can be clearly observed that MLC is able to differentiate snow from all the major glacier terrain classes in the study area and therefore, seems superior to other existing techniques.

Figure 5 shows that classification of only reflectance data leads to precise estimation of snow cover. A comparative evaluation of the three snow-cover maps reveals that while integration of data from sources (i.e., NDSI and thermal data) with reflectance data reduces the misclassification of shadow class (Figures 5b and c) and facilitates the segregation of periglacial and supraglacial debris classes (Figures 5b and d), it does not have much influence on the accuracy of snow-cover mapping.

Thus, these studies clearly demonstrate the potential of per-pixel image classification techniques for snow-cover mapping. However, in per-pixel classification, a pixel is assigned a single class, which may lead to misclassification and misrepresentation of mixed pixels especially in case of coarse spatial resolution data of sensors such as NOAA-AVHRR, Terra-MODIS, IRS-P6-AWiFS, etc. For example, MODIS snow-cover mapping algorithm SNOWMAP classifies a pixel as snow covered if it has at least 60% snow, resulting in over-estimation of snow covered area. Thus, a number of sub-pixel classification techniques for snow-cover mapping have been proposed.

Sub-pixel image classification

The output of a sub-pixel image classification is a set of fraction images equal to the number of classes being mapped. A fraction image is a grayscale image representing pixels values as the proportion of the class to which it belongs. Some sub-pixel classification techniques include MLC in soft form, spectral mixture modeling (SMM) (Settle and Drake, 1993), Fuzzy set–based methods (Bezdek et al., 1984), Evidential Reasoning (ER) (Peddle, 1993), Artificial Neural Networks (ANN) (Foody, 1995), Support Vector Machines (SVMs) (Brown et al., 1999) and Decision-tree classification (Min et al., 2005) etc.

Digital Image Information Extraction Techniques for Snow Cover Mapping from Remote Sensing Data, Table 3 Formulations and descriptions of some supervised and unsupervised image classification algorithms

Classifier	Basic formulations	Description	Supervised	Unsupervised	PP	SP
Parallelepiped Classifier	$\overline{x}_{ck} - S_{ck} \leq DN_{ijk} < \overline{x}_{ck} + S_{ck}$	It defines thresholds for each class (c) using their mean ($\overline{x}_{ck}$) and standard deviation (S_{ck}) in each band (k) and uses these to determine whether a pixel falls in that class.	✓	✗	✓	✗
Minimum Distance to Mean Classifier	Euclidean distance = $d(x,\overline{x_c}) = \left[\sum_{c=1}^{M}(x_c - \overline{x_c})^2\right]^{1/2}$ and $x \in \omega_c$ if $d(x,\overline{x_c})^2 < d\left(x,\overline{x_p}\right)^2$ for all $p \neq c$ where x is a pixel, $\overline{x_c}$ is the mean of the cth class, and ω_c is a set of spectral classes M (total number of spectral classes).	The distances between the pixel to be classified and each class center are compared. The pixel is assigned to the class whose center is the closest to the pixel.	✓	✗	✓	✗
Maximum Likelihood Classifier (MLC)	$p(x/c) = \frac{1}{(2\pi)^{n/2}\lvert\Sigma_c\rvert^{1/2}} e^{\left(-1/2\left[(\mathbf{x}-\overline{x}_c)^T\Sigma_c^{-1}((\mathbf{x}-\overline{x}_c))\right]\right)}$ where $p(x/c)$ is the probability density function of a pixel x as a member of class c, n is the number of bands, $\mathbf{x}$ is the vector denoting spectral response of pixels, $\overline{x}_c$ is the vector of class mean and $\sum_c$ is the variance covariance matrix.	It allocates each pixel to the class with which it has the highest probability of membership and requires the data to follow a normal distribution.	✓	✗	✓	✓

Artificial Neural Network Classifier (ANN)	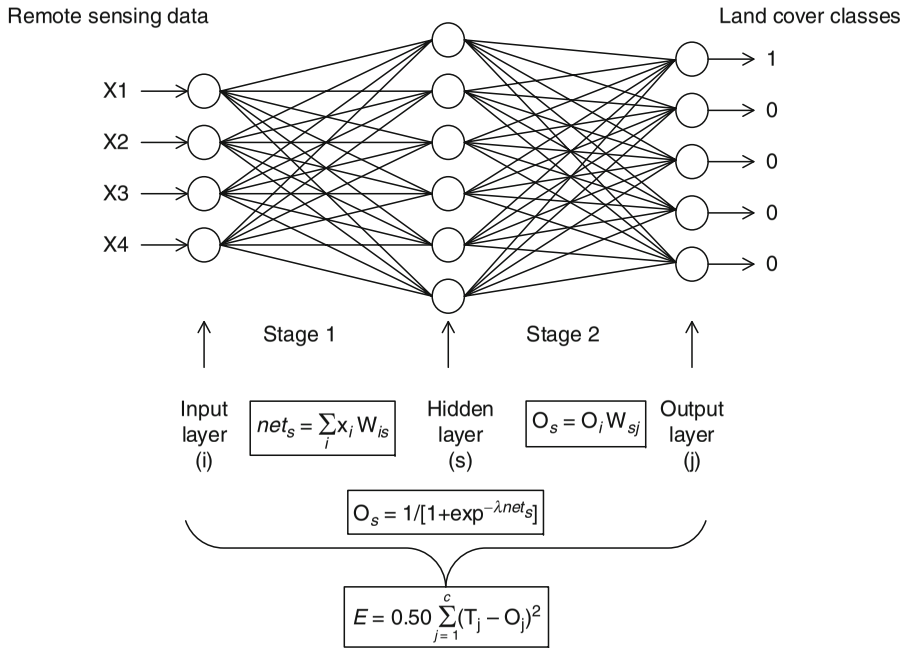	ANN consists of several nodes arranged in three basic layers (input, hidden, and output). The neural network uses the training data to adjust the weights connecting the units until it is able to correctly identify class membership. This is achieved with the aid of an iterative learning process.	✓	✗	✓	✓
	x_i = Input pixel vector; W_{is} = weights between input and hidden l ayer node connections; net_s = net input for hidden layer nodes; O_s = is the output of the sth hidden node. O_j = is the output of the jth unit of the output layer; W_{sj} = weights between hidden and output layer node connections; E = Error function determined from training data and network output. This is to be minimized					
Fuzzy c-Means Clustering Classifier (FCM)	$J_m(U,V) = \sum_{i=1}^{N}\sum_{j=1}^{c} (\mu_{ij})^m \left\|\mathbf{x}_i - v_j\right\|_A^2$ subject to constraints, $\sum_{j=1}^{c} \mu_{ij} = 1$ for all i; $\sum_{i=1}^{N} \mu_{ij} > 0$ for all j; $0 \le \mu_{ij} \le 1$ for all i, j where $\mathbf{x}_i$ is the vector denoting spectral response of a pixel i, V is the collection of vector of cluster centers, v_j, μ_{ij} are class membership values of a pixel (members of fuzzy c-partition matrix), c and N are number of clusters and pixels respectively, m is a weighting exponent ($1 < m < \infty$), $\left\|X_i - v_j\right\|_A^2$ is the squared distance between $\mathbf{x}_i$ and v_j.	FCM measures the fuzzy membership value of data for each cluster based on the distance between the cluster center and the data in the feature space of remotely sensed imagery.	✓	✓	✗	✓

Digital Image Information Extraction Techniques for Snow Cover Mapping from Remote Sensing Data, Table 3 (Continued)

Classifier	Basic formulations	Description	Supervised	Unsupervised	PP	SP
Spectral Mixture Modelling (LMM)	$x_k = \sum_{c=1}^{n} f_c M_{kc} + e_k$ where, M_{kc} is the endmember spectra representing the mean class spectral responses of cth class in kth band, f_c are the fraction of cth class in a pixel, and the term e_k is the error term for kth band, which expresses the difference between the observed spectral response and the model derived spectral response of the pixel, respectively.	It assumes that the spectral response of an individual pixel is a linear sum of the mean spectral responses of its components (i.e. land cover classes) weighted by their relative proportions on the ground and thus calculates the proportion of each class	✓	✗	✗	✓
Evidential Reasoning (ER)	Mass function For one band, the mass function of a class c, for a DN value x is given as, $m_c(x) = \frac{\text{no. of pixels with value } x \text{ intraining sample of class } c}{\text{Total number of pixels intraining sample of class } c}$ Orthogonal summation If m_1 and m_2 are two mass functions defined on inputs from two sources, the combined mass function m_{12} is given by the equations, $m_{12}(A) = \frac{\sum_{B \cap C = A} m_1(B) m_2(C)}{1-k}$ where $A \neq \Phi$ where K is a normalization factor for ignoring conflicting evidence and is mathematically expressed as, $K = \sum_{B \cap C = \Phi} m_1(B) m_2(C)$	The mathematical theory of evidence actually refers to the Dempster–Shafer theory. The theory provides a general heuristic basis for combining information from independent sources, and can be applied to any problem where a choice is to be made from a set of well-known alternatives, based on information from various sources.	✓	✗	✓	✓

Decision Tree Classifier (DT)	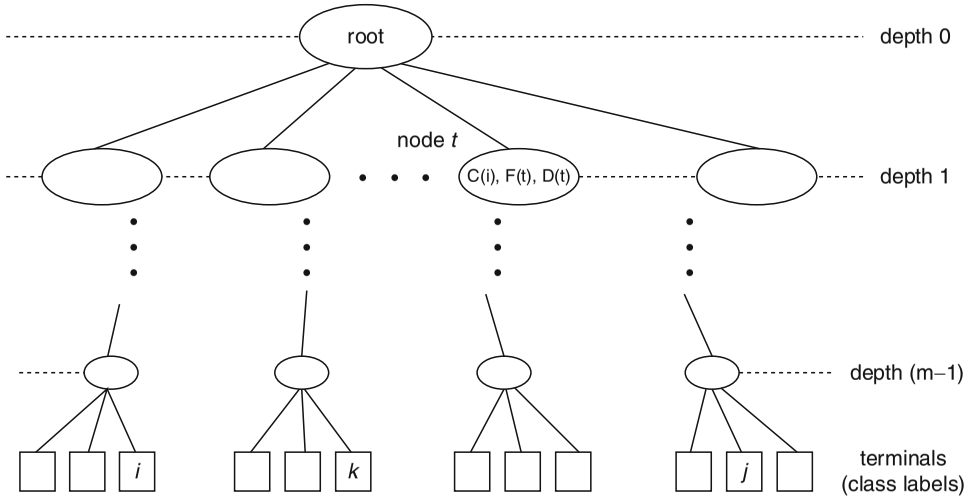 *C*(*t*)- subset of classes accessible from node *t* *F*(*t*)- feature subset used at node *t* *D*(*t*)- decision rule used at node *t*	Decision tree is a nonparametric classifier and involves a recursive partitioning of the feature space, based on a set of rules that are learned by an analysis of the training set. A tree structure is developed where at each branching a specific decision rule is implemented, which may involve one or more combinations of the attribute inputs.	✓	✗	✓
K-Means Clustering	Given a set of observations $(\mathbf{x}_1,\mathbf{x}_2,\ldots,\mathbf{x}_n)$, where each observation is a d-dimensional real vector, then k-means clustering aims to partition this set into k *(M)* partitions ($k < n$) so as to minimize the within-cluster sum of squares : $\underset{\omega}{\operatorname{argmin}} \sum_{c=1}^{k} \sum_{x_c \in \omega_c} \|x_c - \overline{x_c}\|^2$	It is an iterative clustering algorithm. First an arbitrary initial cluster mean vector is assigned. The second step classifies each pixel to the closest cluster mean. In the third step the new cluster mean vectors are calculated based on all the pixels in one cluster. The second and third steps are repeated until the “change” between the iteration is small.	✗	✓	✓

Digital Image Information Extraction Techniques for Snow Cover Mapping from Remote Sensing Data, Table 3 (Continued)

Classifier	Basic formulations	Description	Supervised	Unsupervised	PP	SP
ISODATA	Same as *k*-means with additional merging and splitting of clusters.	The ISODATA algorithm has some further refinements by splitting and merging of clusters. Clusters are merged if either the number of members (pixel) in a cluster is less than a certain threshold or if the centers of two clusters are closer than a certain threshold. Clusters are split into two different clusters if the cluster standard deviation exceeds a predefined value and the number of members (pixels) is twice the threshold for the minimum number of members.	✗	✓	✓	

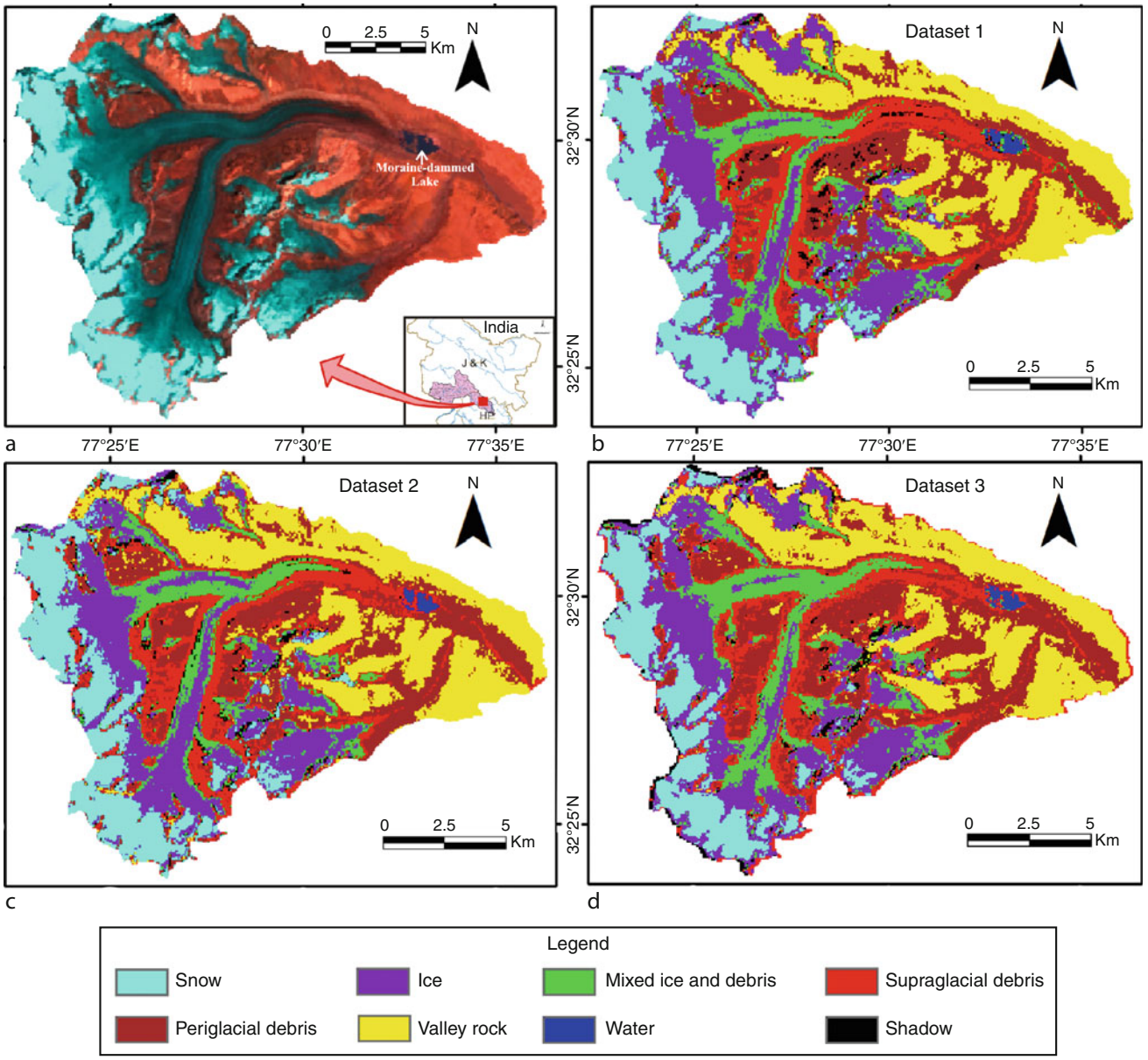

Digital Image Information Extraction Techniques for Snow Cover Mapping from Remote Sensing Data, Figure 5 Snow-cover mapping using per-pixel image classification: **(a)** An FCC (R = B5, G = B4, B = B3) of AWiFS image of a test glacier, **(b)** Glacier terrain map derived from reflectance data, **(c)** Glacier terrain map derived from reflectance data + NDSI, and **(d)** Glacier terrain map derived from reflectance data + thermal data.

Among these, very few have been applied for snow cover estimation. The prevalent approaches of fractional snow-cover mapping include the techniques using empirical relationships (Andersen, 1982; Kaufman et al., 2002; Salomonson and Appel, 2004, 2006), SMM and its variations (Nolin et al., 1993; Painter et al., 2003; Vikhamar and Solberg, 2002, 2003; Sirguey et al., 2008 and 2009), and fuzzy set–based approaches (Rampini et al., 2002). Among all these, SMM has been used most widely in glaciological studies.

Empirical relationships–based snow-cover mapping

In these techniques, an empirical relationship between snow cover and some other property such as reflectance or NDSI, etc., is established, which is used to back calculate the percentage of snow cover in a pixel. Keeping in view the requirements of an operational sub-pixel snow-cover mapping algorithm, techniques based on empirical relationships have been developed (Andersen, 1982; Kaufman et al., 2002; Salomonson and Appel, 2004, 2006). Andersen (1982) developed a fractional snow-cover

mapping algorithm based on an empirical "reflectance to snow-cover" relationship. The model was calibrated by providing two points on the reflectance function: highest reflectance for 0% snow cover, and lower reflectance for 100% snow cover. This algorithm is used by the Norwegian Water Resources and Energy Directorate (NVE) to produce snow-cover maps from NOAA-AVHRR sensor.

Kaufman et al. (2002) devised an empirical technique for the estimation of fractional snow cover, based on principles of remote sensing of aerosol over the land. Both aerosol and sub-pixel snow are dark at 2.1 μm and much brighter at 0.66 μm. A relationship between directional reflectance of the non-snow areas (vegetation and soil) at these wavelengths was used to predict the reflectance at 0.66 μm. The results were validated with the snow fractions obtained from SMM (Rosenthal and Dozier, 1996) as the ground truth. The results showed a difference of only 1–2% between the snow fractions derived from the two techniques.

Salomonson and Appel (2004) conducted a study with the aim to evaluate the utility of NDSI in estimating the fractional snow cover within a 500-m MODIS pixel. For this, the data from Landsat ETM + scenes covering a wide variety of snow cover conditions was acquired as ground truth. All the Landsat scenes were classified as snow or non-snow using the current SNOWMAP algorithm of MODIS. An ordinary least squares regression approach was then applied to derive linear relationships between the snow fraction (FRA) and NDSI corresponding to the 500-m grid cells. Results from this technique proved to be superior, with lowest RMS error in the range of 0.10–0.12 and highest correlation in the range of 0.95–0.97.

Spectral Mixture Modeling

The SMM is widely used for producing class proportions within mixed pixels (Settle and Drake, 1993). SMM models the pixel spectrum with a least squares fit as a linear combination of the spectral responses of classes present within the pixel. The surface spectral responses of classes (also called as endmembers) are thus determined from other sources and the fractional cover of each class is obtained (Konig et al., 2001).

Nolin et al. (1993) were probably the first to apply SMM for mapping fractional snow cover in the mountainous regions of Sierra Nevada, California using AVIRIS data. Two multiband subset images containing 16 and 18 bands in the visible and NIR wavelengths, out of the available 224 bands were used. The SMM was run for each image to calculate the fraction images for each endmember. Deviations between the model and the data were calculated as residuals and RMS error images as well as an overall RMS error were also computed for each image. Overall RMS errors for the two subsets were found to be 3.4 Wm^{-2} μm^{-1} sr^{-1} and 3.0 Wm^{-2} μm^{-1} sr^{-1}, respectively, which are quite low. Therefore, they were able to successfully map deep snow, thin snow, shaded snow, and snow mixed with vegetation.

For operational snow-cover mapping, Rosenthal and Dozier (1996) estimated fractional snow cover using SMM for only a few representative regions and found that the technique was able to accurately identify surfaces without topographic correction (Konig et al., 2001). Recently, Sirguey et al. (2009) have presented a method for production of snow-cover maps with improved spatial resolution of 250 m, using MODIS data, at sub-pixel level. Image fusion techniques (wavelet fusion and "ARSIS" concept, Sirguey et al., 2008) were used to merge the relatively high resolution MODIS band 1 and band 2 (250 m) with MODIS bands 3–7 (500 m) data. A constrained SMM was applied on radiometrically corrected MODIS images. The eight endmembers, namely, ice, debris, rocks, medium granular snow, coarse granular snow, transformed snow, rain-forest + bush, and pasture were identified using ground measurements and photointerpretation. The accuracy of the resultant snow cover fractions was assessed against the reference snow-cover maps derived from fine-resolution ASTER data. The overall RMSE and mean absolute error (MAE) showed an improvement of 25%, while R^2 increased by 5.6% when the MODIS images with improved spatial resolution were used.

Some variations of SMM have also been reported especially in regions of rugged topography through the use of multiple snow endmembers (Painter et al., 2003). A method for sub-pixel mapping of snow cover in forests was developed by Vikhamar and Solberg (2002). The method was based on SMM of snow, trees, and snow-free ground. The focus had been on development of a physically based reflectance model that uses a forest-cover map as prior information. Later they tried to derive a simplified reflectance model suitable for operational snow-cover mapping in forests (Vikhamar and Solberg, 2003).

Although an effective technique, SMM has its own limitations such as that arisen from its basic assumption that the spectral response of a pixel is a linear weighted sum of its constituent classes. Nonlinearities are generated by the adjacency effect of bright pixels (i.e., pixels with high reflectance) next to dark pixels (pixels with low reflectance) adding some unaccounted-for path radiance and by the anisotropic distribution of reflected radiation from snow (particularly in the near-infrared wavelengths), as well as by the presence of adsorbed impurities in snow that can be adequately modeled as an intimate mixture (Nolin et al., 1993). In order to overcome the limitations of SMM, other sub-pixel classification techniques, which account for nonlinearity in spectral mixing have been proposed.

Fuzzy Set–Based Approaches

Fuzzy c-means clustering (FCM) is a popular fuzzy clustering method, which may be employed to partition pixels of remote sensing image into different class membership values or fractions. FCM measures the fuzzy membership value of data for each cluster based on the distance between the cluster center and the data in the feature space

of remotely sensed imagery and may be used in both supervised and unsupervised modes (Table 2). Rampini et al. (2002) used a supervised FCM classifier to extract eight land cover classes (snow, ice, rocks, wood, grass, lakes, clouds, and shadow) from Landsat TM and ETM + images to estimate the changes in the glacier cover from 1986 to 1999. The overall accuracy in all the classes was found to be above 90%.

In order to demonstrate the sub-pixel classification techniques, snow cover was estimated using MLC in soft form, FCM, and Evidential Reasoning (ER) from the AWiFS image in the Chenab basin (Figure 6). The SMM was ruled out due to the constraint that the number of classes to be mapped (eight in present case) should be one less than the number of spectral bands (four in present case of AWiFS data). Visual inspection of the snow cover fraction images from the three classifiers reveals that FCM has been relatively more successful in classifying snow cover as compared to MLC and ER. MLC and ER seem to underestimate and misclassify snow cover.

Summary

Mapping of snow- and ice-covered area has always been one of the major global scientific studies such as the mass balance studies, volumetric estimations of cryospheric components, meltwater runoff modeling, snow hazard prediction modeling, climatological modeling, etc. Conventional snow-cover mapping techniques include ground and aerial surveys, extrapolation of point data from weather stations, from topographic maps, and by application of temperature lapse rate method. The advances in satellite remote sensing have virtually revolutionized the global scenario of cryospheric studies in general, and

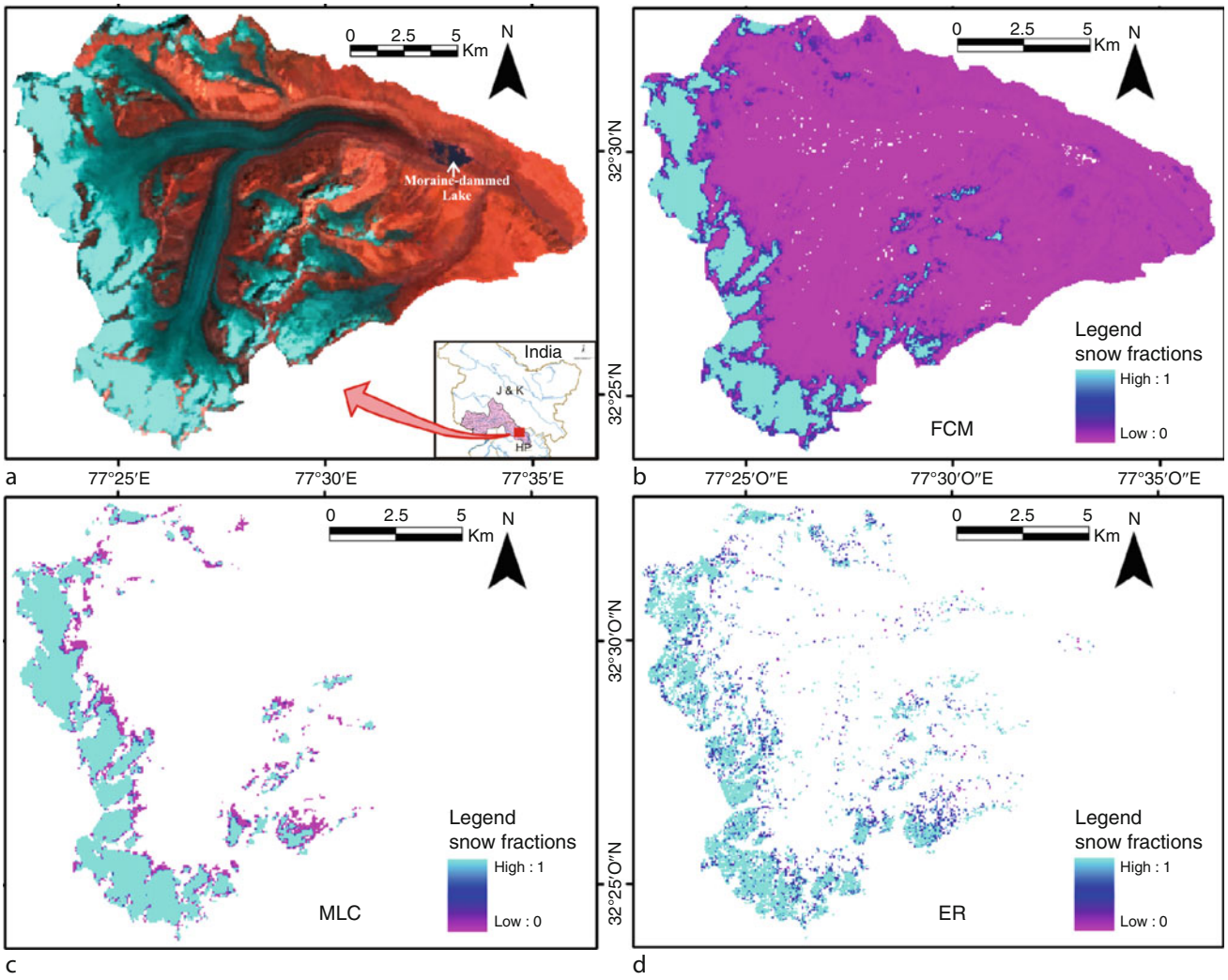

Digital Image Information Extraction Techniques for Snow Cover Mapping from Remote Sensing Data, Figure 6 **(a)** An FCC (R = B5, G = B4, B = B3) of AWiFS image of a test glacier; Pseudo-color snow cover fraction images from **(b)** FCM, **(c)** MLC, and **(d)** ER algorithms.

mapping of snow-covered areas in particular. Parallel to the advancements in the satellite sensor technology and availability of much refined data, the techniques of digital information extraction have also been enhanced. From simple change detection and manual delineation techniques to image ratios, spectral indices, and digital image classification–based mapping of snow-covered areas, there has been an exponential growth in snow-cover mapping at per-pixel and sub-pixel scales. Each technique, discussed in this chapter, has its merits and demerits. For example, while image ratioing and empirical spectral indices are appropriate for operational level tasks, the technically sound methods of digital image classification are more appropriate than others for detailed basin scale studies. Moreover, the results from digital image classification can also be augmented for further improvement by incorporation of data from sources. Moreover, work has also been carried out to exploit potential of the coarse spatial resolution data for snow-cover mapping using sub-pixel techniques, largely based on spectral mixture modeling. The utility of other techniques for snow-cover mapping at operational level needs to be explored. Besides, incorporation of ancillary data at sub-pixel level to enhance the classification accuracy and moving from sub-pixel classification to sub-pixel mapping or "super resolution mapping" of snow-covered areas constitute some areas for future research.

Conclusively, it may be stated that rapidly advancing tool of remote sensing has yet not reached its zenith and would continue to evolve and grow and in order to keep pace with it and imbibe its advantages in the field of snow-cover mapping.

Bibliography

Allen, N. W., and Mosher, F. R., 1985. Interactive snow cover mapping with geostationary satellite data over the western United States. In *Summaries, 19th International Symposium on Remote Sensing of Environment*, Ann Arbor, Michigan, p. 153.

Andersen, T., 1982. Operational snow mapping by satellites. In *Hydrological aspects of Alpine and high mountain areas. Proceedings of the Exeter Symposium*, July 1982. Wallingford: IAHS Publ. 138, pp. 149–154.

Aniya, M., Sato, H., Naruse, R., Skvarca, P., and Casassa, G., 1996. The use of satellite and airborne imagery to inventory outlet glacier of Southern Patagonian Icefield, South America. *Photogrammetric Engineering and Remote Sensing*, **62**, 1361–1369.

Bamber, J., 2006. Remote sensing in glaciology. In Knight, P. G. (ed.), *Glacier Science and Environmental Change*. Malden, MA: Wiley, 527 p.

Baumgartner, M. F., and Rango, A., 1991. Snow cover mapping using microcomputer image processing systems. *Nordic Hydrology*, **22**, 193–210.

Berthier, E., Arnaud, Y., Kumar, R., Ahmad, S., Wagnon, P., and Chevallier, P., 2007. Remote sensing estimates of glacier mass balances in the Himachal Pradesh (Western Himalaya, India). *Remote Sensing of Environment*, **108**(3), 327–338.

Bezdek, J. C., Ehrlich, R., and Full, W., 1984. FCM: The fuzzy c-means clustering algorithm. *Computers and Geosciences*, **10**, 191–203.

Binaghi, E., Madella, P., Montesano, M. P., and Rampini, A., 1997. Fuzzy contextual classification of multisource remote sensing images. *IEEE Transactions on Geoscience and Remote Sensing. GE-35*, **2**, 326–339.

Bronge, L. B., and Bronge, C., 1999. Ice and snow type classification in Vestfold Hills, East Antarctica, using LANDSAT TM data and ground radiometer measurements. *International Journal of Remote Sensing*, **20**(2), 225–240.

Brown, M., Gunn, S. R., and Lewis, H. G., 1999. Support vector machines for optimal classification and spectral unmixing. *Ecological Modelling*, **120**, 167–179.

Della Ventura, A., Rampini, A., Rabagliati, R., and Serandrei-Barbero, R., 1983. Glacier monitoring by satellite. *Il Nuovo Cimento, C-1*, **6**, 211–221.

Della Ventura, A., Rampini, A., and Serandrei-Barbero, R., 1987. Development of a satellite remote sensing technique for the study of alpine glaciers. *International Journal of Remote Sensing*, **8**, 203–215.

Dozier, J., 1989. Spectral signature of alpine snow-cover from the Landsat Thematic Mapper. *Remote Sensing of Environment*, **28**, 9–22.

Ehrler, C., and Seidel, K., 1995. Mutual effects of the climate change and the alpine snow cover and their influence on the runoff regime evaluated with the aid of satellite remote sensing. In Stein, T. I. (ed.), *IGARSS'95; Quantitative Remote Sensing for Science and Applications*. Italy: Florence, Vol. 3, pp. 1973–1975.

Foody, G. M., 1995. Land cover classification by an artificial neural network with ancillary information. *International Journal of Remote Sensing*, **16**, 527–542.

Foster, J. L., Hall, D. K., and Chang, 7., 1987. Remote sensing of snow. *Eos, Transaction of the American Geophysical Union*, **68**(32), 682–684.

Fukushima, Y., Watanabe, O., and Higuchi, K., 1991. Estimation of streamflow change by global warming in a glacier-covered high mountain area of the Nepal Himalaya. In Proceedings of Bergmann, H., Lang, H. P., Frey, W., Issler, D., and Salm, B. (eds.), *International symposium snow, hydrology and forests in high alpine areas Vienna*, August 11 –24, 1991. International association of hydrological sciences. IAHS/AISH Publication, 205, pp. 181–188.

Gratton, D. J., Howarth, P. J., and Marceau, D. J., 1990. Combining DEM parameters with Landsat MSS and TM imagery in a GIS for mountain glacier characterization. *IEEE Transactions on Geoscience and Remote Sensing*, **28**, 766–769.

Gupta, R. P., 2003. *Remote Sensing Geology*, 2nd edn. Berlin: Springer Publication, p. 655.

Gupta, R. P., Haritashya, U. K., and Singh, P., 2005. Mapping dry/wet snow cover in the Indian Himalayas using IRS multispectral imagery. *Remote Sensing of Environment*, **97**(4), 458–469.

Haeberli, W., Hoelzle, M., and Suter, S., 1998. Into the second century of worldwide glacier monitoring: prospects and strategies. *A contribution to the International Hydrological Programme (IHP) and the Global Environment Monitoring System (GEMS), UNESCO Studies and Reports in Hydrology*, 56, 228 p.

Haeberli, W., Kääb, A., Vonder Mühll, D., and Teysseire, P., 2001. Prevention of outburst floods from periglacial lakes at Grubengletscher, Valais, Swiss Alps. *Journal of Glaciology*, **47**(156), 111–122.

Hall, D. K., Ormsby, J. P., Bindschadler, R. A., and Siddalingaiah, H., 1987. Characterization of snow and ice zones on glaciers using Landsat Thematic Mapper data. *Annals of Glaciology*, **9**, 104–108.

Hall, D. K., Chang, A. T. C., and Siddalingaiah, H., 1988. Reflectances of Glaciers as calculated from the Landsat 5 Thematic Mapper data. *Remote Sensing of Environment*, **25**, 311–321.

Hall, D. K., Riggs, G. A., and Salomonson, V. V., 1995a. Development of methods for mapping global snow-cover using moderate

resolution spectroradiometer data. *Remote Sensing of Environment*, **54**, 127–140.

Hall, D. K., Benson, C. S., and Field, W. O., 1995b. Changes of glaciers in Glacier Bay, Alaska, using ground and satellite measurements. *Physical Geography*, **16**(1), 27–41.

Hall, D. K., Foster, J. K., Verbyla, D. L., Klein, A. G., and Benson, C. S., 1998. Assessment of snow-cover mapping accuracy in a variety of vegetation-cover densities in Central Alaska. *Remote Sensing of Environment*, **66**(2), 129–137.

Hall, D. K., Kelly, R. EJ., Foster, J. L., and Chang, A. T. C., 2005. Estimation of snow extent and snow properties. In Anderson, M. G., (eds.), *Encyclopedia of Hydrological Sciences.* New York: Wiley, pp. 811–828.

Holroyd, E. W., Verdin, J. P., and Carroll, T. R., 1989. Mapping snow cover with satellite imagery: comparison of results from three sensor systems. In *Proceedings of the 57th Annual Western Snow Conference*, Ft. Collins, Colorado, pp. 59–68.

IPCC, 2007. Climate Change 2007: The physical science basis. In Solomon, S., Qin, D., Manning, M., Chen, Z., Marquis, M., Averyt, K. B., Tignor, M., and Miller, H. L. (eds.), *Contribution of Working Group I to the Fourth Assessment Report of the Intergovernmental Panel on Climate Change*. Cambridge: Cambridge University Press, 996 pp.

Jacobs, J. D., Simms, E. L., and Simms, A., 1997. Recession of the southern part of Barnes Ice Cap, Baffin Island, Canada, between 1961 and 1993, determined from digital mapping of Landsat TM. *Journal of Glaciology*, **43**(143), 98–102.

Justice, C. O., Wharton, S. W., and Holben, B. N., 1981. Application of digital terrain data to quantify and reduce the topographic effect on Landsat data. *International Journal of Remote Sensing*, **2**(3), 213–230.

Kaufman, Y. J., Kleidman, G. R., Hall, D. K., Martins, J. V., and Barton, J. S., 2002. Remote Sensing of sub-pixel snow-cover using 0.66 and 2.1 m channels. *Geophysical Research Letters*, **29**(16), 28–1–28–4.

Keshri, A., Shukla, A., and Gupta, R. P., 2009. ASTER ratio indices for supraglacial terrain mapping. *International Journal of Remote Sensing*, **30**(2), 519–524.

Khromova, T. E., Osipova, G. B., Tsvetkov, D. G., Dyurgerov, M. B., and Barry, R. G., 2006. Changes in glacier extent in the eastern Pamir, Central Asia, determined from historical data and ASTER imagery. *Remote Sensing of Environment*, **102** (1–2), 24–32.

Klein, A. G., Hall, D. K., and Riggs, G. A., 1998. Improving snow-cover mapping in forests through the use of caopy reflectance model. *Hydrological Processes*, **12**, 1723–1744.

Knap, W. H., and Reijmer, C. H., 1998. Anisotropy of the reflected radiation field over melting glacier ice: measurements in Landsat TM bands 2 and 4. *Remote Sensing of Environment*, **65**, 93–104.

Konig, M., Winther, J. G., and Isaksson, E., 2001. Measuring snow and glacier ice properties from satellite. *Reviews of Geophysics*, **39**(1), 1–27.

Kulkarni, A. V., Singh, S. K., Mathur, P., and Mishra, V. D., 2006. Algorithm to monitor snow cover using AWiFS data of RESOURCESAT-1 for the Himalayan region. *International Journal of Remote Sensing*, **27**(12), 2449–2457.

Kulkarni, A. V., Bahuguna, I. M., Rathore, B. P., Singh, S. K., Randhawa, S. S., Sood, R. K., and Dhar, S., 2007. Glacier retreat in Himalayas using Indian Remote Sensing satellite data. *Current Science*, **92**(1), 69–74.

Liang, T., Zhang, T., Xie, H., Wu, C., Feng, Q., Huang, Q., and Chen, Q., 2008. Toward improved daily snow cover mapping with advanced combination of MODIS and AMSR-E measurements. *Remote Sensing of Environment*, **112**(10), 3750–3761.

Lillesand, T. M., Meisner, D. E., LaMois-Downs, A., and Denell, R. L., 1982. Use of GOES and TirosINOAA satellite data for snow cover mapping. *Photogrammetric Engineering and Remote Sensing*, **48**(2), 251–259.

Miller, D. H., 1953. Snow cover depletion and runoff. *Snow Hydrology.* Portland: U. S Army Corps of Engineers.

Min, X., Watanachaturaporn, P., Varshney, P. K., and Arora, M. K., 2005. Decision tree regression for soft classification of remote sensing data. *Remote Sensing of Environment*, **97**(3), 322–336.

Nolin, A., and Liang, S., 2000. Progress in bidirectional reflectance modelling and application for surface particulate media: snow and soils. *Remote Sensing Reviews*, **14**, 307–342.

Nolin, A. W., Dozier, J., and Mertes, L. A. K., 1993. Mapping alpine snow using spectral mixture modeling technique. *Annals of Glaciology*, **17**, 121–124.

Oerlemans, J., Dyurgerov, M., and Van de Wal, R. S. W., 2007. Reconstructing the glacier contribution to sea-level rise back to 1850. *The Cryosphere Discuss*, www.the-cryospherediscuss.net/1/77/2007/, **1**: 77–97.

Painter, T. H., Dozier, J., Roberts, D. A., Davis, R. F., and Green, R. O., 2003. Retrieval of sub-pixel snow covered area and grain size from imaging spectrometer data. *Remote Sensing of Environment*, **85**, 64–77.

Paul, F., 2000. Evaluation of different methods for glacier mapping using Landsat TM. *EARSEL eProceedings*, **1**, 239–244.

Paul, F., 2003. *The new Swiss glacier inventory 2000: application of remote sensing and GIS*. PhD thesis. Zürich, Department of Geography, University of Zürich, 198 pp.

Paul, F., Kääb, A., Maisch, M., Kellenberger, T., and Haeberli, W., 2002. The newremote-sensing-derived Swiss glacier inventory: I Methods. *Annals of Glaciology*, **34**, 355–361.

Paul, F., Kääb, A., Maisch, M., Kellenberger, T., and Haeberli, W., 2004. Rapid disintegration of Alpine glaciers observed with satellite data. *Geophysical Research Letters B*, **31**(21), L21402, doi:10.1029/2004GL020816.

Peddle, D. R., 1993. An empirical comparison of evidential reasoning, linear discriminate analysis and maximum likelihood algorithm for Alpline land cover classification. *Canadian Journal of Remote Sensing*, **19**, 31–42.

Potts, H. L., 1944. A photographic survey method of forecasting runoff. *Transactions – American Geophysical Union*, **25**(1), 153–194.

Quincey, D. C., Lucas, R. M., Richardson, S. D., Glasser, N. F., Hambrey, M. J., and Reynolds, J. M., 2005. Optical remote sensing techniques in high-mountain environments: application to glacial hazards. *Progress in Physical Geography*, **29**(4), 475–505.

Racoviteanu, A. E., Williams, M. W., and Barry, R. G., 2008. Optical remote sensing of glacier characteristics: a review with focus on the Himalaya. *Sensors*, **8**, 3355–3383.

Rampini, A., Brivio, P. A., Rota Nodari, F., and Binaghi, E., 2002. Mapping Alpine glaciers changes from space. *IEEE Transactions on Geoscience and Remote Sensing Symposium*, 2199–2201.

Rango, A., and Martinec, J., 1981. Accuracy of snowmelt runoff simulation. *Nordic Hydrology*, **12**, 265–274.

Riggs, G. A., Hall, D. K., and Salomonson, V. V., 1994. A snow index for the Landsat thematic mapper and moderate resolution imaging spectroradiometer. In *Proceedings of the International Geoscience and Remote Sensing Symposium, IGARSS '94*, August 8–12, 1994, Pasadena, CA, pp. 1942–1944.

Riggs, G. A., Hall, D. K., and Salomonson, V. V., 1996. Recent progress in development of the moderate resolution imaging spectroradismeter snow cover algorithm and product. In *Proceedings of the International Geoscience and Remote Sensing Symposium, IGARSS '96*, Lincoln, NE, pp. 139–141.

Rosenthal, W., and Dozier, J., 1996. Automated mapping of montane snow-cover at sub-pixel resolution from the Landsat Thematic Mapper. *Water Resources Research*, **100**, 115–130.

Rott, H., and Markl, G., 1989. Improved snow and glacier monitoring by the Landsat Thematic Mapper. In *Proceedings of a workshop on the Landsat Thematic Mapper applications,* ESA SP-1102, pp. 3–12.
Saito, A., and Yamazaki, T., 1999. Characteristics of spectral reflectance for vegetation ground surfaces with snowcover: Vegetation indices and snow indices. *Journal of Japan Society of Hydrology and Water Resources*. **12**, 28–38.
Salomonson, V. V., and Appel, I., 2004. Estimating fractional snowcover from MODIS using the normalised difference snow index. *Remote Sensing of Environment*, **89**, 351–360.
Salomonson, V. V., and Appel, I., 2006. Development of the Aqua MODIS NDSI fractional snow cover algorithm and validation results. *IEEE Transactions on Geoscience and Remote Sensing*, **44**(7), 1747–1756.
Settle, J. J., and Drake, N. A., 1993. Linear mixing and the estimation of ground cover proportions. *International Journal of Remote Sensing*, **14**, 1159–1177.
Shi, J., and Dozier, J., 1997. Mapping seasonal snow with SIR-C/X-SAR in mountainous areas. *Remote Sensing of Environment*, **59**(2), 294–307.
Shimamura, Y., Izumi, T., and Matsumaya, H., 2006. Evaluation of a useful method to identify snow-covered areas under vegetation – comparisons among a newly proposed snow index, normalized difference snow index and visible reflectance. *International Journal of Remote Sensing*, **27**(21), 4867–4884.
Shiyin, L., Wenxin, S., Yongping, S., and Gang, L., 2003. Glacier changes since the Little Ice Age maximum in the western Qilian Shan, northwest China, and consequences of glacier runoff for water supply. *Journal of Glaciology*, **49**, 117–124.
Sidjak, R. W., and Wheate, R. D., 1999. Glacier mapping of the Illecillewaet icefield, British Columbia, Canada, using Landsat TM and digital elevation data. *International Journal of Remote Sensing*, **20**(2), 273–284.
Singh, P., and Singh, V. P., 2001. *Snow and Glacier Hydrology.* The Netherlands: Kluwer Academic Publishers, pp. 742.
Sirguey, P., Mathieu, R., Arnaud, Y., Khan, M. M., and Chanussot, J., 2008. Improving MODIS spatial resolution for snow mapping using wavelet fusion and ARSIS concept. *IEEE Geoscience and Remote Sensing Letters*, **5**(1), 78–82.
Sirguey, P., Mathieu, R., and Arnaud, Y., 2009. Subpixel monitoring of the seasonal snow cover with MODIS at 250 m spatial resolution in the Southern Alps of New Zealand: methodology and accuracy assessment. *Remote Sensing of Environment*, **113**, 160–181.
Solberg, R., Malnes, E., Amlien, J., Koren, H., Eikvil1, L., and Storvold, R., 2005. Multi-sensor/multi-temporal approaches for snow cover area monitoring. In *Proceedings of EARSeL LIS-SIG Workshop,* Berne, February, 2005.
Tait, A. B., Hall, D. K., Foster, J. L., and Armstrong, R. L., 1999. Utilizing multiple datasets for snow-cover mapping. *Remote Sensing of Environment*, **72**, 111–126.
Tarble, R. D., 1963. Areal distribution of snow as determined from satellite photographs. *IAHS Publication*, **65**, 372–375.
Vikhamar, D., and Solberg, R., 2002. Subpixel mapping of snow cover in forests by optical remote sensing. *Remote Sensing of Environment*, **84**, 69–82.
Vikhamar, D., and Solberg, R., 2003. Snow-cover mapping in forests by constrained linear spectral unmixing of MODIS data. *Remote Sensing of Environment*, **88**, 309–323.
Wang, J., and Li, W., 2003. Comparison of methods of snow cover mapping by analyzing the solar spectrum of satellite remote sensing data in China. *International Journal of Remote Sensing*, **24**(21), 4129–4136.
Warren, S. G., 1982. Optical properties of snow. *Reviews of Geophysics*, **20**(1), 67–89.
Warren, S. G., and Wiscombe, W. J., 1980. A model for the spectral albedo of snow, II, Snow containing atmospheric aerosols. *Journal of Atmospheric Sciences*, **37**, 2734–2745.
Williams, R. S., Jr., and Hall, D. K., 1993. Glaciers. In Gurey, R. J., Foster, J. L., and Parkinson, C. L. (eds.), *Atlas of Satellite Observations Related to Global Change*. Cambridge: Cambridge University Press, 401–421.
Williams, R. S., Hall, D. K., and Benson, C. S., 1991. Analysis of glacier facies using satellite techniques. *Journal of Glaciology*, **37**, 120–128.
Williams, R. S. Jr., Hall, D. K., Sigurdsson, O., and Chein, J. Y. L., 1997. Comparison of satellite-derived with ground- based measurements of the fluctuations of the margins of Vatnajokull, Iceland, 1973–1992. *Annals of Glaciology*, **24**, 72–80.
Winther, J. G., and Hall, D. K., 1999. Satellite derived- snow coverage related to hydropower production in Norway: present and future. *International Journal of Remote Sensing*, **20**(15–16), 2991–3008.
Winther, J. G., Gerland, S., Orback, J. B., Ivanov, B., Blanco, A., and Boike, J., 1999. Spectral reflectance of melting snow in a high Arctic watershed on Svalbard: some implications for optical satellite remote sensing studies. *Hydrological Processes*, **13**(12–13), 2033–2049.
Wiscombe, W. J., and Warren, S. G., 1980. A model for the spectral albedo of snow, I, Pure snow. *Journal of Atmospheric Sciences*, **37**, 2712–2733.
Xiao, X., Shen, Z., and Qin, X., 2001. Assessing the potential of VEGETATION sensor data for mapping snow and ice cover: a normalized difference snow and ice index. *International Journal of Remote Sensing*, **22**(13), 2479–2487.
Zeng, Q., Cao, M., Feng, X., Liang, F., Chen, X., and Sheng, W., 1984. A study of spectral reflection characteristics for snow, ice and water in the north of China. In *Hydrological Applications of Remote Sensing and Remote Data Transmission: Proceedings of the Hamburg Symposium.* Wallingford, UK: IAHS Publ. 145, pp. 451–462.

DIRECT SURFACE RUNOFF

Lars Bengtsson
Department of Water Resources Engineering, Lund University, Lund, Sweden

Definition

Direct surface runoff is the rain or meltwater that runs off during the rain or melt event as overland flow or in the vegetation cover above a frozen soil.

The meltwater and the rain falling onto snow or on frozen ground reach a stream along different pathways. It may be as groundwater after vertical infiltration in macropores or through the soil matrix. It may be as saturated overland flow or as Hortonian overland flow on concrete frozen soil; or as flow in cracks just below the ground surface. The water reaching a stream during or just after snowmelt or after a storm event may be old subsurface water forced forward by new water, or it may be event water, that is, meltwater or event rain water. The quality of the stream water depends on the pathways and on the interactions with the soil during the particles route to the stream.